Available online at www.sciencedirect.com
SCIENCE DIRECT®
Journal of Molecular Catalysis A: Chemical 229 (2005) 25–29
JOURNAL OF MOLECULAR CATALYSIS A: CHEMICAL
www.elsevier.com/locate/molcata

CO oxidation and NO reduction over supported Pt-Rh and Pd-Rh nanocatalysts: a comparative study

Abir De Sarkar, Badal C. Khanra*

Condensed Matter Physics Group, Saha Institute of Nuclear Physics, 1/AF, Bidhannagar, Calcutta 700064, India

Received 5 March 2004; received in revised form 26 October 2004; accepted 26 October 2004
Available online 10 December 2004

Abstract

The surface compositions of supported $Pt_{50}Rh_{50}$ and $Pd_{50}Rh_{50}$ three-way catalysts (TWC) have been simulated by Monte-Carlo (MC) technique and used for calculating the activity of the catalysts for CO oxidation and NO reduction. Pd-Rh shows a higher activity than Pt-Rh for CO oxidation in presence of O_2, while Pt-Rh is a better CO oxidation catalyst in absence of O_2. For NO reduction, Pt-Rh nanoparticles are better catalysts both in presence and absence of O_2. β-N_2 is found to be the most dominant channel for N_2 formation on Pt-Rh nanoparticles, while, δ-N_2 is found to be the most dominant pathway for N_2 production on Pd-Rh. The poisoning effect of sulphur is found to be more on Pd-Rh catalyst than on Pt-Rh catalyst.

Keywords: Nanocatalysts; Monte-Carlo (MC) simulation; Microkinetic model; Three-way catalysts

1. Introduction

The use of Pt-Rh/CeO_2-Al_2O_3 formulations as three-way catalysts (TWC) has been known to be very effective in controlling the emission of polluting gases into the environment [1–7]. These catalysts convert simultaneously CO, NO and unburnt hydrocarbons (HC) into harmless gases like CO_2, N_2 and H_2O. Requirements of stricter control over emissions and the high temperature durability of the catalysts have led to improved formulation like Pt-Rh/CeO_2-ZrO_2-Al_2O_3, where the supports CeO_2-ZrO_2-Al_2O_3 show improved control over the oxygen supply for the reactions, high temperature durability (up to 1100 K) and the ability to minimize the deactivation of the catalysts by sulphur and other impurities present in the fuel [4,5]. Market price of the precious metals Pt and Rh has necessitated partial substitution of Pt by Pd. However, for substituting Pd for Pt in the commercial TWC formulation, the fuel must have little or no Pb and sulphur content. Besides, Pd segregates as PdO on the Pd–Rh alloy surface under oxidising condition up to temperatures 1000 K, where PdO decomposes [3]. The surface segregation of Pd in Pd-Rh catalysts suppresses the NO_x reduction. It is the purpose of the present work to see how the segregation behaviour of Pd-Rh nanoparticles differs from that for Pt-Rh nanocatalysts, and how the segregation behaviour and the presence of sulphur in the fuel affects the CO oxidation and NO reduction on the two catalysts.

We have used the Monte-Carlo (MC) simulation to predict the surface composition of $Pt_{50}Rh_{50}$ and $Pd_{50}Rh_{50}$ particles having in total 2406 atoms—the diameter of the particles being of the order of 4 nm. For simplicity, we have considered the particles to have the fcc cubo-octahedral structure as all the three metals have the fcc crystal structure, and for particles of such sizes, cubo-octahedral geometry has the higher stability. A brief discussion on the MC model and the simulated surface composition results are presented in Section 2. For comparing the activities of the Pt-Rh and Pd-Rh nanocatalysts for the $CO + O_2$, $CO + NO$ and $CO + NO + O_2$ reactions, we use a microkinetic model. A brief discussion of the microkinetic model and the computed activities of the two cata-

* Corresponding author. Tel.: +91 33 2337 5345; fax: +91 33 2337 4637.
E-mail address: badal@cmp.saha.ernet.in (B.C. Khanra).

1381-1169/$ – see front matter © 2004 Elsevier B.V. All rights reserved.
doi:10.1016/j.molcata.2004.10.052

lysts are presented in Section 3. Conclusions are drawn in Section 4.

2. MC simulation and surface segregation in Pt-Rh and Pd-Rh nanocatalysts

In the MC simulation scheme [8–10], one determines the pair bond energy between two nearest neighbour atoms, E_{ij}, as

$$E_{ij} = \frac{w_{ij}}{Z} + \frac{E_c^i(n)}{n} + \frac{E_c^i(m)}{m} \quad (1)$$

where the indices i and j indicate the atoms A or B of the bimetallic system AB, w_{ij} the interchange energy for two dissimilar atoms and Z is the bulk coordination number. $E_c^i(n)$ is the partial bond energy of the ith atom with n nearest neighbours, and is estimated from the empirical formula:

$$E_c^i(n) = a^i + b^i n + c^i n^2. \quad (2)$$

a^i, b^i and c^i in (2) are the adjustable parameters derived from the experimental data of dimer energy, surface energy and the cohesive energy of a metal. With the computed pair bond energy, E_{ij}, one can find the equilibrium configuration energy and the resulting surface composition. The values of the parameters used for the present MC simulations are the following [10,11]:

Pt: $a = -0.4287398$, $b = -0.0474969$, $c = 0.0035483$,

Pd: $a = -0.17702$, $b = -0.04842$, $c = 0.002987$,

Rh: $a = -0.4744544$, $b = -0.0341727$, $c = 0.0028138$,

and

$$\frac{w_{ij}}{Z(\text{Pt-Rh})} = -0.00691\,\text{eV}; \qquad \frac{w_{ij}}{Z(\text{Pd-Rh})} = -0.00396\,\text{eV},$$

The MC-simulated fractions of Pt (Pd) atoms dispersed on the 2406-atom supported Pt-Rh and Pd-Rh nanoparticles are shown in Fig. 1. It may be noticed that almost 95% of Pd-Rh particle surface is covered with Pd atoms, while the Pt-Rh surface is only mildly enriched in Pt (≈55% of surface covered by Pt atoms). The segregation behaviour as found in our MC simulation is quite understandable if one considers the relative values of the heat of sublimation and the surface free energies of the three transition metals [11]. The lattice strain energies will have only a very marginal effect on segregation behaviour of these systems. Though it is possible to calculate the surface composition of smaller or larger particle sizes, the overall results would change insignificantly for particle sizes of catalytic interest having diameter larger than 3 nm [8,9]. The temperature range 450–675 K is considered

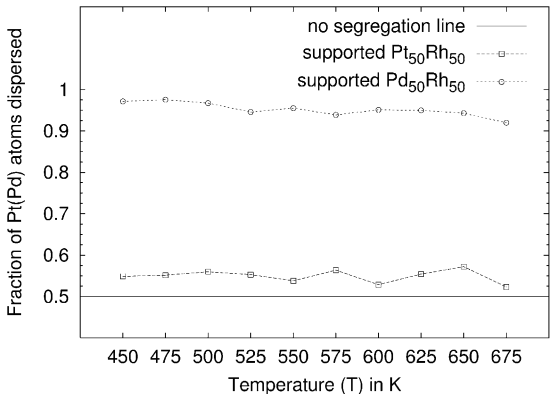

Fig. 1. MC-simulated fraction of Pt (Pd) atoms dispersed on 2406-atom cubo-octahedral $Pt_{50}Rh_{50}$ and $Pd_{50}Rh_{50}$ nanoparticles as a function of temperature.

in this work as this is the temperature range where CO oxidation and NO reduction reactions take place in the catalytic converter. The predicted segregation behaviour agrees well with available experimental results on supported Pt-Rh [12] and Pd-Rh particles [13].

3. Microkinetic analysis of CO + O_2, CO + NO and CO + NO + O_2 reactions

The microkinetic analysis is made in three stages. In Stage I, we formulate the elementary reaction steps that are to be considered for the overall reactions leading to the formation of CO_2 and N_2 molecules. For our studies, we consider the following elementary steps:

(i) adsorption and desorption of CO and NO,
(ii) dissociative adsorption of O_2 molecule,
(iii) dissociation of molecularly adsorbed NO into adsorbed atomic nitrogen and oxygen atom,
(iv) formation of N_2 molecules through two possible steps, namely, $N_a + N_a \rightarrow N_2$ (the β-N_2 molecule) and $NO_a + N_a \rightarrow N_2 + O_a$ (the δ-N_2 molecule), where the subscript 'a' indicates the adsorbed species, and finally,
(v) formation of CO_2 molecules through the combination of adsorbed CO and adsorbed O.

In Stage II, the rates of the elementary steps are determined. For example, the rate of adsorption of CO, NO and O_2 on a metal m may be given by molecular collision theory as [14–17]

$$(r_{a,i})_m = \left(\frac{RT}{2\pi M_i}\right)^{1/2} \sigma_m (S_i)_m C_i \theta_v \quad (3)$$

where M_i is the molecular weight of the adsorbed species i, σ_m the area occupied by 1 mol of surface atoms (cm^2/mol) of the metal m, $(S_i)_m$ is the initial sticking coefficient of the species i on the metal m; C_i is the concentration of the component i in the gas phase. θ_v is the fraction of va-

cant surface sites available for adsorption and is given by $\theta_v = 1-\theta_{CO}-\theta_{NO}-\theta_N-\theta_O-\theta_S$.

Similarly, the rates of desorption of CO and NO may be expressed as [14–16]

$$r_{d,CO} = A\ \exp\left[-\frac{E-\alpha_{CO}\theta_{CO}-\alpha_N\theta_N}{RT}\right]\theta_{CO} \quad (4)$$

and

$$r_{d,NO} = A\ \exp\left[-\frac{E}{RT}\right]\theta_{NO}, \quad (5)$$

respectively. In the expressions (4) and (5), A's are the pre-exponential factors (s^{-1}), E's the activation barriers (kcal/mol) for CO and NO desorptions and α_{CO} and α_N are the CO_a-CO_a and CO_a-N_a repulsive energies (kcal/mol), respectively.

Likewise, the rate of NO dissociation may be given by

$$r_{diss,NO} = A\ \exp\left(-\frac{E}{RT}\right)\theta_{NO}\theta_v, \quad (6)$$

and rates for β-N_2 and δ-N_2 formation are given by

$$r_{N_2,\beta} = A\ \exp\left(-\frac{E-\alpha_N\theta_N}{RT}\right)\theta_N^2 \quad (7)$$

and

$$r_{N_2,\delta} = A\ \exp\left(-\frac{E}{RT}\right)\theta_{NO}\theta_N, \quad (8)$$

respectively. α_N in Eq. (7) represents the repulsive interaction between two adsorbed N atoms. For the rate of an elementary reaction on the AB alloy particle, we use the approximation $r_{AB} = (x_s)_A r_A + [1-(x_s)_A]r_B$, where $(x_s)_A$ is the surface concentration of A atoms on the surface of the AB particle. The surface composition may be obtained from the MC simulation results of Section 2. The data required for these rates are provided in Table 1.

Finally, in Stage III, one solves self-consistently the steady-state continuity equations for the adsorbed species CO_a, NO_a, N_a and O_a and determines the turnover numbers (TON) of CO_2 and N_2 molecules molecules (defined as the number of CO_2 or N_2 molecules released per site per second) [14–16]. It may be mentioned here that this microkinetic analysis would, in general, predict results experimentally obtainable from flow type reactors.

In Fig. 2, we compare the TON of CO_2 on Pt-Rh and Pd-Rh particles for the three reactions. It may be noticed that while for $CO + O_2$ and $CO + NO + O_2$ reactions, Pd-Rh is a better oxidation catalyst; for the $CO + NO$ reaction, Pt-Rh is a better catalyst for the CO oxidation. Furthermore, it may also be noticed in Fig. 2 that the light-off temperature, i.e. the minimum temperature at which the conversion starts taking place, is higher for the $CO + NO$ reaction than for the $CO + O_2$ and $CO + NO + O_2$ reactions. This is true for both the bimetallic systems. From Fig. 3, we may conclude that for NO reduction, Pt-Rh is a better catalyst than Pd-Rh. In Fig. 4, we have shown for the $CO + NO$ reaction, the contribution of δ-N_2 and β-N_2 to the total turnover number of N_2 molecules on Pt-Rh catalysts. They are compared with the TON of CO_2 molecules. Two important features may be noticed in Fig. 4. First, the TON of CO_2 is marginally higher than the TON of N_2. Secondly, the contribution of δ-N_2 molecules to total N_2 produc-

Table 1
Parameter values used in model calculations for $CO + NO + O_2$ reaction

	Pt [17,18]	Rh [15]	Pd [19,20]
CO adsorption			
σ_m	4.03	3.75	3.60
S_{CO}	0.50	0.50	0.96
CO desorption			
A	1.0	16.0	10.0
E	29.63	31.6	34.0
α_{CO}	6.5	4.5	5.0
α_N	–	10	–
CO_2 formation			
A	1.0	0.1	0.1
E	13.5	14.3	25
NO adsorption			
S_{NO}	0.5	0.5	0.3
NO desorption			
A	5	5	5
E	26	26	32
NO dissociation			
A	0.003	0.003	0.04
E	29	19	27.7
O_2 adsorption			
S_O	0.012	0.01	0.4
δ-N_2 formation			
A	–	0.0002	–
E	–	21	–
β-N_2 formation			
A	0.013	0.003	0.003
E	20.2	31	32.5
α_N	–	4	–

Units: σ_m (in 10^8 cm^2/mol); E, α (in kcal/mol); A (in 10^{13} s^{-1}).

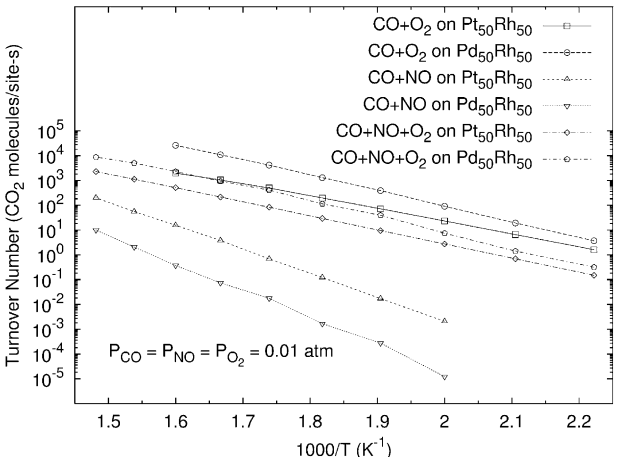

Fig. 2. Turnover number of CO_2 molecules as a function of temperature for $CO + O_2$, $CO + NO$ and $CO + NO + O_2$ reactions on Pt-Rh and Pd-Rh catalysts.

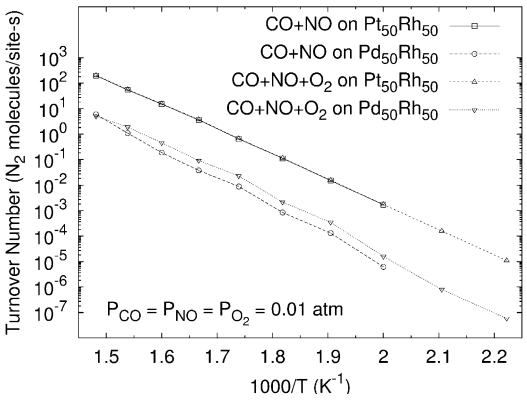

Fig. 3. Turnover number of N_2 molecules as a function of temperature for CO + NO and CO + NO + O_2 reactions on Pt-Rh and Pd-Rh catalysts.

tion is much less compared to that of β-N_2 molecules. This signifies that N_2 molecules are mainly formed by combination of adsorbed *N* atoms, which in turn, result from dissociation of NO molecules. From similar CO + NO reaction studies on Pd-Rh catalyst, it has been found that δ-N_2 molecules mainly contribute to total N_2 production—signifying that N_2 is formed from the dissociation of N_2O into N_2 and O. In case of CO + NO + O_2 reaction, the nature of contributions of δ-N_2 and β-N_2 molecules to the total TON of N_2 molecules on the two catalysts has been found to be similar to the case of CO + NO reaction. However, because of the availability of excess oxygen for these reactions, the TON of CO_2 molecules is much higher than the TON of N_2 molecules. This is true for both the catalysts.

We have also studied the role of sulphur in poisoning the reactions on the two catalysts. Pd is known to be more sensitive to poisons like lead and sulphur [21,22]. A microkinetic analysis of the activities of the supported Pt-Rh and Pd-Rh catalysts confirms this observation as may be seen from Fig. 5. In Fig. 5(a), we have plotted for the two catalysts turnover numbers of CO_2 molecules as a function of sulphur coverage, θ_s. It may be noticed that for the Pd–Rh system, an increase of sulphur coverage from 0 to 0.16 leads to a drop in TON by

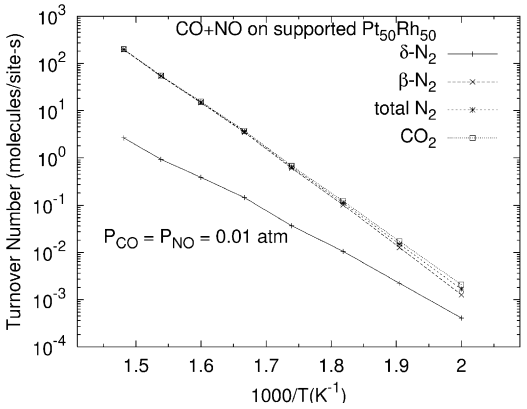

Fig. 4. Turnover number of β-N_2, δ-N_2, N_2 and CO_2 as a function of temperature for CO + NO reaction on $Pt_{50}Rh_{50}$ catalysts.

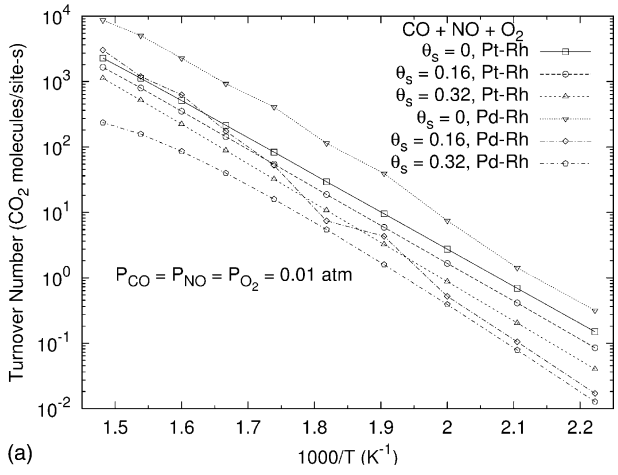

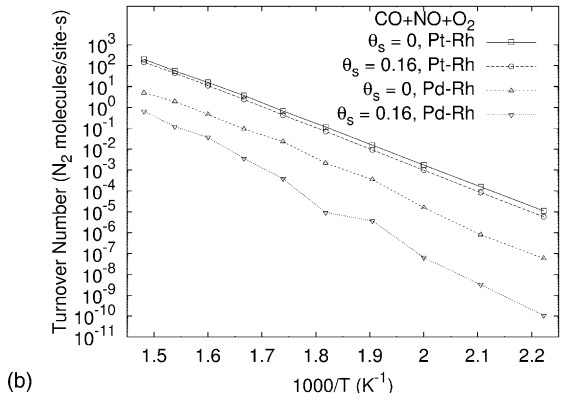

Fig. 5. Turnover numbers from CO + NO + O_2 reaction on supported Pt-Rh and Pd-Rh catalysts as a function of temperature and sulphur coverage: (a) CO_2 molecules and (b) N_2 molecules.

more than an order of magnitude throughout the temperature range of 450–675 K. But, for the Pt–Rh system, the drop in TON of CO_2 is much less [23]. For the sulphur coverage of 0.32, the TON of CO_2 decreases further in the case of both the catalysts.

In Fig. 5(b), we have shown the role of sulphur on the TON of N_2 molecules on the two catalysts. It may be seen that TON of N_2 is severely affected on Pd-Rh catalysts compared to Pt-Rh catalysts. The results, shown in Fig. 5, thus indicate that sulphur poisons the Pd-Rh catalysts more than the Pt-Rh catalysts.

As mentioned earlier in Section 2 that for particles having diameter larger than 3 nm, the surface composition changes insignificantly with particle size, the activity is also expected to behave in a similar fashion. The experimental results are, however, scarce to verify this theoretical prediction.

4. Conclusions

CO oxidation and NO reduction on Pt, Rh and Pt–Rh bimetallic surfaces have been studied exhaustively both experimentally as well as theoretically. However, studies on

supported Pd-Rh are scarce. This led us to use theoretical models to study the two systems under identical conditions.

A comparison is made here of the activities of the supported $Pt_{50}Rh_{50}$ and $Pd_{50}Rh_{50}$ nanocatalysts for the $CO + O_2$. $CO + NO$ and $CO + NO + O_2$ reactions. Our investigations led to the following results:

1. Pt and Pd are found to segregate to the surfaces of the $Pt_{50}Rh_{50}$ and $Pd_{50}Rh_{50}$ particles, respectively, but the extent of Pd segregation to the surface of $Pd_{50}Rh_{50}$ is very high compared to the Pt segregation in $Pt_{50}Rh_{50}$.
2. Pd-Rh is a better catalyst for CO oxidation, while Pt-Rh is a better catalyst for NO reduction.
3. N_2 formation on Pt-Rh catalyst takes place principally via the β-N_2 route, whereas on Pd-Rh catalyst, it is the δ-N_2 route by which N_2 is formed.
4. For the $CO + NO + O_2$ reaction, the rate of CO_2 formation is higher than the rate of N_2 formation on both the catalysts, while, for the $CO + NO$ reaction, the rates are closer.
5. The kinetic behaviour of $CO + NO + O_2$ reaction is closer to that of $CO + O_2$ reaction than to the $CO + NO$ reaction.
6. The presence of NO inhibits the light-off temperature. The light-off temperature for $CO + NO$ reaction is much higher than that of $CO + NO + O_2$ and $CO + O_2$ reactions.
7. For both the CO oxidation and the NO reduction reaction, sulphur poisons the Pd-Rh catalyst more than the Pt-Rh catalyst.

Acknowledgments

B.C.K. thanks Professor Y. Iwasawa for his suggestion to study the poisoning effect of sulphur on the two catalysts.

References

[1] K.C. Taylor, Catal. Rev.-Sci. Eng. 35 (1993) 457.
[2] K.C. Taylor, Automotive Catalytic Converters, Springer, Berlin, 1984.
[3] H.S. Gandhi, G.W. Graham, R.W. McCabe, J. Catal. 216 (2003) 433.
[4] J. Kaspar, P. Fornasiero, N. Hickey, Catal. Today 77 (2003) 419.
[5] J. Kaspar, P. Fornasiero, M. Graziani, Catal. Today 50 (1999) 285.
[6] D.R. Monroe, M.H. Krueger, D.D. Beck, M.J. D'Aniello Jr., in: A. Crucq (Ed.), Catalysis and Automotive Pollution Control II, Elsevier, Amsterdam, 1991, p. 593.
[7] D.D. Beck, J.W. Sommers, in: A. Frennet, J.-M. Bastin (Eds.), Catalysis and Automotive Pollution Control III, Elsevier, Amsterdam, 1995, p. 721.
[8] T.S. King, R.G. Donnely, Surf. Sci. 141 (1984) 417.
[9] A.M. Schoeb, T.H. Raeker, L. Yang, X. Wu, T.S. King, A.E. DePristo, Surf. Sci. Lett. 278 (1992) L125.
[10] A. De Sarkar, B.C. Khanra, Chem. Phys. Lett. 353 (2002) 426.
[11] F.R. de Boer, R. Boom, W.C.M. Mattens, A.R. Miedema, A.K. Niessen, Cohesion in Metals, North-Holland, Amsterdam, 1988, and references therein.
[12] N. Savargaonkar, B.C. Khanra, M. Pruski, T.S. King, J. Catal. 162 (1996) 277.
[13] G.W. Graham, T. Potter, R.J. Baird, H.S. Gandhi, M. Shelef, J. Vac. Sci. Technol. A 4 (3) (1996) 1613.
[14] S.H. Oh, C.C. Eickel, J. Catal. 112 (1988) 543.
[15] S.H. Oh, G.B. Fisher, J.E. Carpenter, D.W. Goodman, J. Catal. 100 (1986) 360.
[16] S.H. Oh, J.E. Carpenter, J. Catal. 101 (1986) 114.
[17] R.K. Herz, S.P. Marin, J. Catal. 65 (1980) 281.
[18] Th. Fink, J.P. Dath, R. Imbihl, G. Ertl, J. Chem. Phys. 95 (1991) 2109.
[19] T. Engel, G. Ertl, J. Chem. Phys. 69 (1978) 1267.
[20] S.M. Vesecky, D.R. Rainer, D.W. Goodman, J. Vac. Sci. Technol. A 14 (1996) 1457.
[21] T. Maillet, J. Barbier Jr., P. Gelin, H. Praliaud, D. Duprez, J. Catal. 202 (2001) 367.
[22] J.A. Rodriguez, T. Jirsak, S. Chaturvedi, J. Chem. Phys. 110 (1999) 3138.
[23] A. De Sarkar, B.C. Khanra, Chem. Phys. Lett. 384 (2004) 339.